



Citation for published version:

Soleimani, M & Rymarczyk, T 2023, 'Ultrasound tomography for lung imaging: an experimental phantom study', *IEEE Sensors Journal*, vol. 23, no. 8, pp. 8769-8775. <https://doi.org/10.1109/JSEN.2023.3252340>

DOI:

[10.1109/JSEN.2023.3252340](https://doi.org/10.1109/JSEN.2023.3252340)

Publication date:

2023

Document Version

Peer reviewed version

[Link to publication](#)

© 2023 IEEE. Personal use of this material is permitted. Permission from IEEE must be obtained for all other uses, in any current or future media, including reprinting/republishing this material for advertising or promotional purposes, creating new collective works, for resale or redistribution to servers or lists, or reuse of any copyrighted component of this work in other works.

University of Bath

Alternative formats

If you require this document in an alternative format, please contact:
openaccess@bath.ac.uk

General rights

Copyright and moral rights for the publications made accessible in the public portal are retained by the authors and/or other copyright owners and it is a condition of accessing publications that users recognise and abide by the legal requirements associated with these rights.

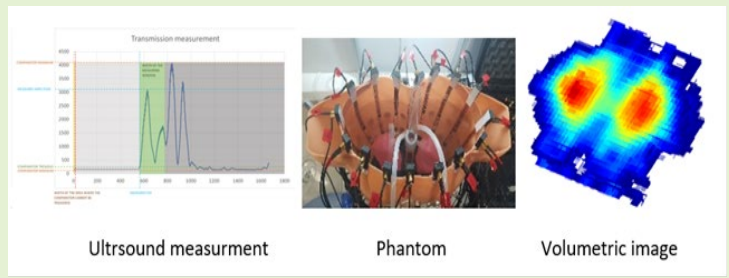
Take down policy

If you believe that this document breaches copyright please contact us providing details, and we will remove access to the work immediately and investigate your claim.

Ultrasound tomography for lung imaging: an experimental phantom study

Manuchehr Soleimani¹, Tomasz Rymarczyk²

Abstract— The ability to create real-time images of pulmonary function is highly desirable in many clinical situations. For example, information on air delivery is vital for patients in the intensive care unit who are going through mechanical ventilation due to respiratory failure. The functional information obtained from imaging can be used to provide early warnings of developing pulmonary pathologies in real-time, reducing complications and improving patient outcomes. Electrical impedance tomography (EIT) is an imaging system that has gone through clinical studies and provides such information. EIT has several drawbacks the most important one is its limited spatial resolution and very low resolution in depth, which can not be avoided by adding more electrodes. Therefore, it is possible to introduce ultrasound tomography (UST) as an imaging technique with the potential to provide real-time non-ionizing pulmonary monitoring in lung imaging. In contrast, the UST can show significant resolution enhancement when more transducers are used. The central region of thorax can be detected with UST due to its enhanced resolution in central area. In this work, we developed a realistic geometry thorax phantom and are focusing on the performances of 3D UST for lung imaging applications. Results are validated using experimental thoracic phantoms representing the possible use of UST for lung imaging. The UST imaging is achieved by detecting and reconstructing the changes of sound velocity distribution resulting from pulmonary functions and conditions.



Index Terms—Ultrasound Tomography (UST); Lung imaging; Pulmonary function; TOF imaging;

I. Introduction

Ultrasound tomography (UST) has been successfully developed for breast cancer imaging [1]. UST works by interrogating a medium for its speed of sound and/or sound amplitude decays, revealing the medium's acoustical properties. It is non-invasive and non-destructive, compatible with a highly dynamic situation such as lung imaging. UST reconstructs the sound velocity distribution from the measurement of time of flight from an array transducers between transmitters and receivers. Tomographic algorithms make it a robust method and can mitigate the challenge aroused by the complexity of ultrasound propagation in complicated media. The acoustic velocity is sensitive to the contents of gas, liquid, and their distribution, because of the contrast in their acoustic properties. Thus, it is possible to monitor the amount of gas and fluid in the thorax by reconstructing the sound velocity distribution, which can be useful in many diseases. It gives ultrasound-based imaging an advantage over traditional imaging methods such as computed tomography (CT) and magnetic resonance imaging (MRI). However, very detailed resolution of cancerous tissues, such as the one in breast cancer

imaging, needs many UST transducers. A UST with a fast imaging rate is needed to establish a UST device for bedside lung function imaging. Hence in this work, we propose a 32-channel UST system for volumetric lung imaging.

Ultrasound is applied to heart imaging [2], liver [3], brain [4] and many other human organs [5]. In most of these situations, the imaging is done by transmitting ultrasound at a high frequency of around MHz into the human body, and the images are based on reflected signal. However, reflection imaging is hard to create in lung imaging because complex reflection and refraction occur at the thorax [6]. Additionally, the high frequency will rapidly attenuate the acoustic wave, resulting in the reflected signal's low signal-to-noise ratio (SNR). State-of-the-art thoracic imaging methods include X-ray CT, MRI, and electrical impedance tomography (EIT) [7]. Each one of these methods has major limitations. The radiation from CT and X-rays harms human health and cannot be used in long-term monitoring. The equipment of MRI is not portable, so it cannot be used at the bedside. The air in the lung makes the MRI images of lower quality than other organs. The

Paper submitted on xxxxx.

M. Soleimani is with the Electrical and Electronic Engineering Department, University of Bath, UK. (e-mail: m.soleimani@bath.ac.uk)

Tomasz Rymarczyk is with Research & Development Centre Netrix S.A. & WSEI University, Lublin, Poland. (e-mail: tomasz@rymarczyk.com)

resolution of EIT is relatively low, and the EIT cannot provide information in the central area of imaging.

The thorax model is established and verified by simulations and experiments for sound propagation in the low-frequency range [8,9]. While the sound of frequency between 1 and 10 kHz is hard to go through the human thorax. Ultrasound with a frequency between 10 kHz and 700 kHz can penetrate the human thorax. An ultrasound system at this band permits monitoring of the human pulmonary system. As stated, the reflection imaging will require high frequency and is not useable in lung monitoring.

On the other hand, the transmission ultrasound data can be useful in diagnosing various lung diseases and functions, see [8,9,10]. The transmission ultrasound signal can also be used to conduct travel time tomography. Travel time tomography for the thorax has not been well studied. There are no experimental studies related to lung UST imaging. This is despite great progress made in further advancement of the UST devices and algorithms in past few years [11-14]. A simulations study of thorax UST was shown in [15].

In patients undergoing mechanical ventilation because of respiratory failure, there are limited or no real-time imaging tools indicating pulmonary function. A bedside imaging system that visualizes the lung in revisualizesn be lifesaving. Real-time images could provide early warnings of developing pulmonary pathologies in real-time, thereby reducing the incidence of complications and improving patient outcomes. A low-frequency UST is an imaging technique with the potential to provide real-time non-ionizing pulmonary monitoring in the ICU setting. In this paper, we show the results of a new phantom study with 32-senor array UST sensors in two rings of 16 sensors allowing for real-time 3D imaging of air volume in a simple lung phantom. Lung UST application is dynamic imaging, so many transducers generally used in other medical applications of UST may provide challenges in data collection and image reconstruction. However, the proposed UST system is both low costs and computationally cost-effective making it a good candidate for bedside imaging. We provide results of air volume reconstruction using a multi-modality UST dynamical reconstruction algorithm.

The paper is organized as follows. Section II presents the phantom design and the principle of 3D UST reconstruction used in this study. Section III presents static and dynamic experiments. Moreover, finally, in section IV, conclusions are drawn.

II. UST SYSTEM AND METHOD

This section describes the UST system and sensor setup used in this study. Moreover, describe the image reconstruction algorithm used for volumetric UST imaging. Fig. 1 shows the two rings of transducers at 40 kHz central frequency placed around the chest phantom. Additionally, the EIT electrodes are also positioned in the same two rings. This allows for some comparison between two modalities.

A. Thorax phantom

A special chest phantom was prepared for the examination. The structure of the lungs is quite complicated. A simplified version was created for laboratory purposes. The prepared models retain the shape of the lungs but do not consider the

more complicated structures, surfaces and parts of the lungs. First, a model of the right lung was made. Each lung has a separate flexible tube that pumps air into it. It stimulates the trachea. The model of the left lung is smaller than the right one, just like a natural human lung, where the left lung is smaller to make room for the heart in the chest. Because the lungs are not symmetrical, they differ in size, shape, and detail, which is why they were modeled that way. In the model structure, brackets were inserted at the arms' height for the electrodes' attachment. The bottom of the phantom was glued in several stages to strengthen and seal it.

EIT electrodes were made of graphite with a diameter of 4 mm. They were placed on laminated copper tapes and secured with plastic sleeves. PCBs with 2×16 SMB sockets were made. PCBs were milled and mounted on laminated tapes and connected to graphite electrodes. The housings cover the SMB sockets and are a mounting bracket for the complete electrode. 16 pcs of complete, double electrodes were mounted around the perimeter of the phantom. The distance of the lower electrode from the bottom is approx. 80 mm. Assembly elements were made with a frame for assembling artificial lungs with the possibility of replacing the phantoms and adjusting the height. A device for powering the phantom lungs was also prepared. A platform for the resuscitator was made, in which a motor with gear was used. The pumping speed (frequency) is controlled by the PWM controller. The device is powered by DC 12V/2A.

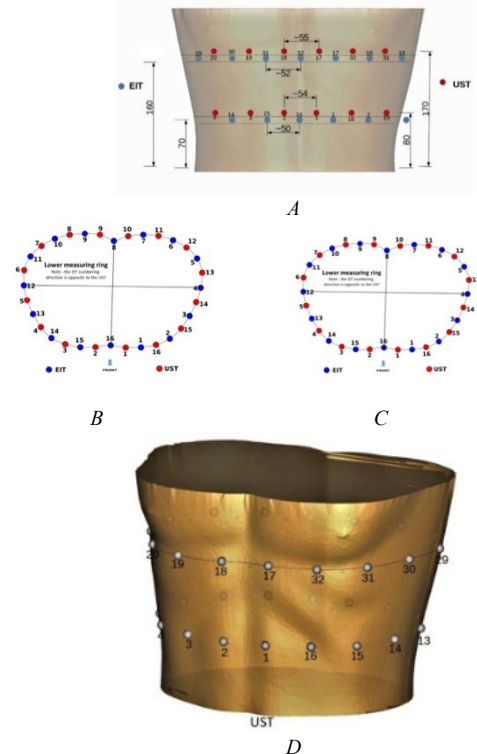


Fig. 1. (A) Two rings of 16 UST transducers; (B) top plane with EIT sensors, (C) bottom plane with EIT sensors, (D) the UST sensors

B. UST hardware

The ultrasonic tomograph has 32 independently working channels that can perform measurements in transmission and reflection modes. This paper uses 32 channel sensors in a single plan 3D USCT mode (Fig. 2).

The device consists of eight four-channel measurement cards, and the FD connects the CAN bus with the measurement module. The measuring module combines a microprocessor measuring system with a touch panel and control application. It also supervises measurement sequences, controls the high-voltage converter, stores configuration parameters and switches USB HS buses.

Parameters of the UST tomograph used during examinations:

- Signal forcing (square bipolar signal $\pm 72V$, maximum current efficiency 3A)
- Max single channel sampling rate: 4MBPS
- Analog signal filtering: band-pass filter with 40kHz center frequency and 50kHz bandwidth
- Adjustable analogue gain :
 - o Stage analog +7.5dB to +55.5dB
 - o Stage II: from +6dB to +36dB
- Analog processing of the signal to the envelope (3-step sensitivity adjustment)
- Apache Kafka Ethernet communication

A waterproof ceramic ultrasonic transducer with the following parameters: $f=40kHz$, $f_i=14mm$, $h=9mm$ was used for the measurements.



Fig. 2. UST tomograph and the UST transducer

The key elements of our tomograph are measurement cards (Fig. 3). They consist of the STM32G474 microcontroller, LM2940S LDO stabilizer, FDCAN1 bus, LR low-pass filter with cut-off frequency (-3dB) around 1 MHz, MCP664 (60MHz) and TL974 (12MHz) measuring amplifiers and the OPA355 operational amplifier operating in the adder circuit. The card has a 5-bit addressing switch, allowing addresses from 0 to 63. The area of the four-channel pulser is shielded with an apulseally-made cover with an inner layer of copper tape. The analogue modules have shianalogovers the cards do not have built-in high-voltage converters. Therefore, an additional board

with a high-voltage section powering the entire set of measurement cards was made. The device has an independent FDCAN2 on which communication between individual modules is carried out.



Fig. 3. 3D model of the ultrasound card

The high-voltage converter module has two isolated DC-DC converters, NMT0572SC, with the possibility of changing the positive and negative voltage using relays. (+24V, -24V, +48V, -48V, +72V, -72V). In addition, the converters were protected with miniature slow-blow fuses (Fig. 4). The high-voltage converter module is an additional extension board of the main module mounted on four spacer sleeves. There is also a small audio amplifier on the board, amplifying the sound from the 8-bit synthesizer built into the FT811 display, which was used to play short characteristic sound signals.



Fig. 4. High-voltage converter on the board of the control module

The main module contains the STM32H743ZI microprocessor supporting CAN FD 8MBPS buses. The board allows the connection of micro SD cards and has a battery backup for the RTC clock and FRAM memory. The FDCAN, SPI, and RS485 buses are led out through the connector in the RJ45 standard cat. 6a.

Parameters used for measurements of the torso phantom:

- Number of channels: 16 one-ring + 16-second ring
- Force frequency: 40kHz
- Number of pulses: 6
- Force signal voltage: $\pm 72V$
- Gain: 44.3 dB
- Filtering: 40kHz bandpass filter and 50kHz bandwidth activated
- Convert to envelopes: running
- The measurements taken are: TOF and amplitude

- Measurement sensors: UST transducers (mounted on the torso - measurements with pink lung phantoms) - 40kHz MCUSD14A40S09RS-30C diameter 14mm

Performing a measurement using UST consists of cyclical sending of a signal from one sensor and measurement on the other probes. The measurement of one frame is completed after all sensors receive the signal. Then the signal is sent from the next probe and received on the other sensors. This sequence is repeated for all probes. Each transducer can work as a transmitter and as a receiver of ultrasonic waves. Individual measurements are transferred to the UST scanner controller. The resulting measurement is stored in the appropriate data matrix. The device in the TOF measurement mode performs 8192 signal samples on each channel, which corresponds to 2.048ms. TOF value is calculated through a calibrated method. The sampling interval of the 4MBPS ADC is 0.25us and can be taken as the accuracy level of TOF calculations.

Fig. 5 shows background TOF data measurement from 32 channel system. A plastic rod in the central area is holding the two balloons and the reference data includes this rod.

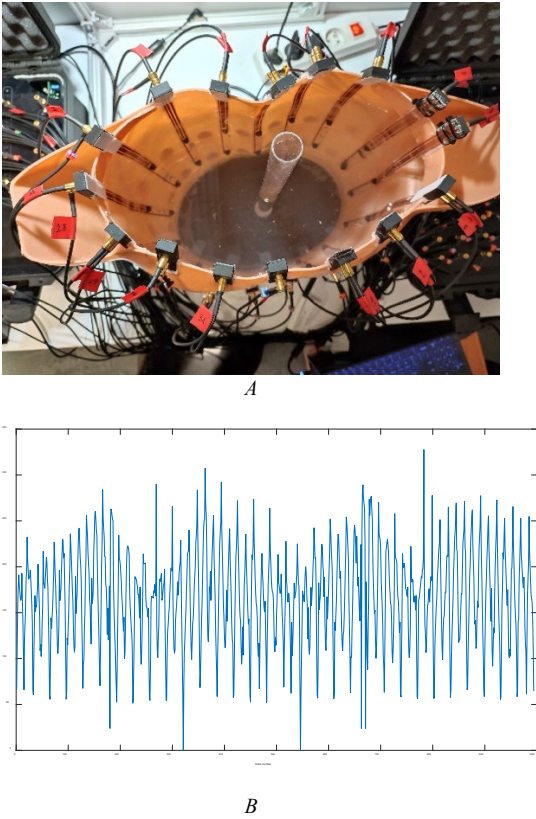


Fig.5 Background measurement TOF data

Sensors within a 120-degree angle of the transmitting probe are used as meaningful data for transmitting mode UST. Fig. 6 shows the signal-to-noise ratio for those usable data, leading to an average of 67 dB.

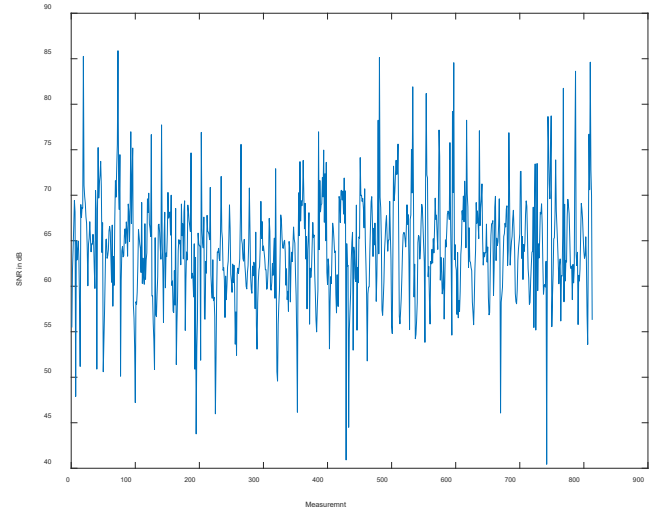


Fig. 6. Signal-to-noise ratio

C. UST Image reconstruction

Transmission signals are the direct travel time from the transmitter to the receivers. The image reconstruction is generated by using time difference imaging, collecting background data (reference data), TOF_b , and the data (data collected by scanning a changing medium), TOF_i . TOF measurement data, is the travel-time delays (μs), eq. (1).

$$\Delta M = TOF_i - TOF_b \quad (1)$$

In UST the travel time data is collected for all transmitter and receiver combinations So ΔM stands for TOF data for all possible measurements. A generalized tomographic forward operator can be expressed as:

$$\Delta M = A \Delta S + e \quad (2)$$

Where ΔS is the reconstructed distribution based on acoustic features, A is the modeling operator, which expresses the sensitivity distribution in the FOV, ΔM is the sensor's recorded data, and e is the noise in the measurements. A ray-based method was used to generate the sensitivity matrix, as shown in [11]. A simplified inversion can be done using back projection.

$$\Delta S \approx A^T \Delta M \quad (3)$$

Total Variation regularisation (TV) [16] was used, showing an efficient method for the regularised inverse problem. The TV problem is defined as an optimization problem, minimizing

$$\|A \Delta S - \Delta M\|^2 + a \|\nabla \Delta S\|_1 \quad (4)$$

optimization parameter, ∇ is the gradient and $\|\cdot\|_1$ is the l_1 -norm. Then the problem to be solved is the constrained optimisation problem, as shown in eq. (5).

$$x_a = \arg \min_{\Delta S} \left(\alpha \|\nabla \Delta S\|_1 \right) \text{ such that} \quad (5)$$

$$\|A \Delta S - \Delta M\|^2 < p,$$

where p is determined based on our knowledge of measurement noise

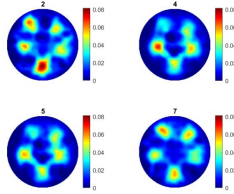
It is solved by the Split Bregman-based TV algorithm [12]. Then, carefully choosing the regularisation parameter, we optimize the image by deleting undesired artifacts. The image reconstruction is a volumetric reconstruction and deals with two rings as a single 3D imaging problem.

III. EXPERIMENTAL RESULTS

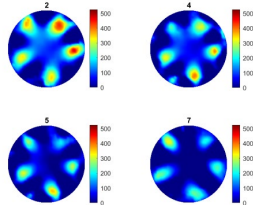
The EIT is the bedside imaging used for lung imaging. It is possible that the UST could offer many advantages over EIT if it can be deployed in thoracic imaging. Here we highlight one of those issues, low image resolution in a central area for EIT. To indicate how the EIT and UST may differ, we provide two example experiments with a cylindrical tank phantom. As it can be seen, while the reconstruction of the boundary inclusions is similar for both imaging systems (Fig. 7), the UST can recover the interior inclusion in Fig. 8.



A



B

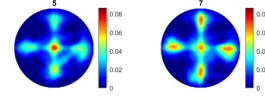
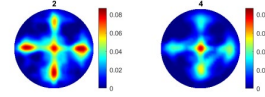


C

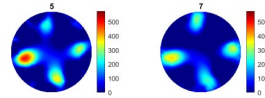
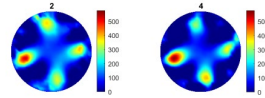
Fig. 7 Cylindrical phantom with two rings of 16 channels for UST and EIT, five inclusions. A) Phantom, B)UST, C)EIT



A



B

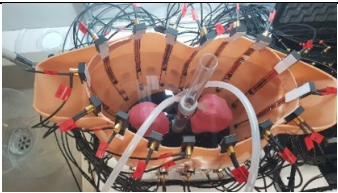
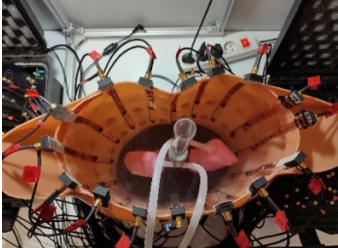
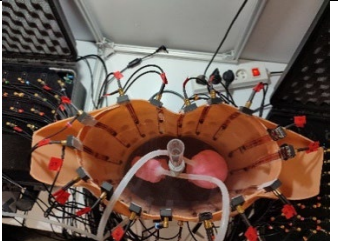


C

Fig. 8 Cylindrical phantom with two rings of 16 channels for UST and EIT, five inclusions. A) Phantom, B)UST, C)EIT

Several static and dynamic measurements of the lung phantom were made. Table 1 shows the list of representative static experiments shown here.

Table 1: Static experiments

Experiments	Phantom
Both side filled (Fig. 9)	
Air is removed from both sides (Fig. 10)	
Left has air removed (Fig. 11)	

Static experiments include Fig. 9, where the two balloons are filled with air. The true phantom and a cross-section image in the middle plane from volumetric image are shown, and a 3D UST system reconstructs a volumetric representation of the air volume. Fig.10 shows an experiment in that air was removed from both balloons. It can be seen from the size of the air volume reconstruction and scale bar in the image compared with Fig. 9 representing the air removal. In Fig. 11, the air was removed from the left balloon, as it is reconstructed from the reconstructed UST images.

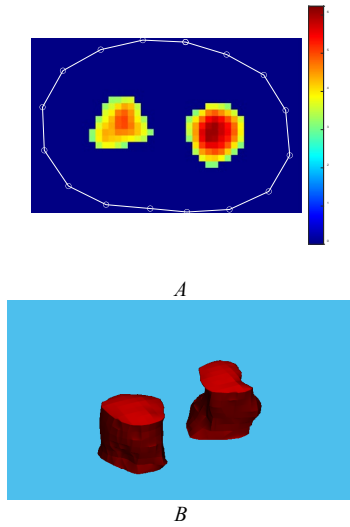


Fig.9 Equal air on both sides. A) Image slice in a midplane, B)Volume plot

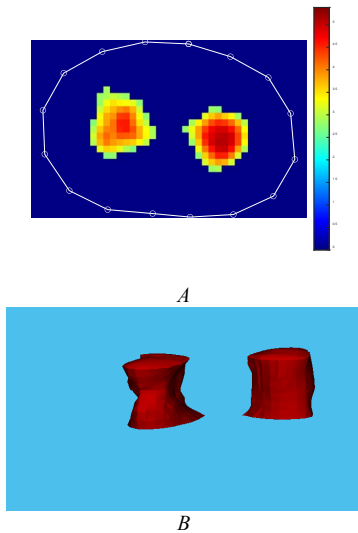


Fig.10 Removing air from both sides, A) Image slice in midplane, B)Volume plot

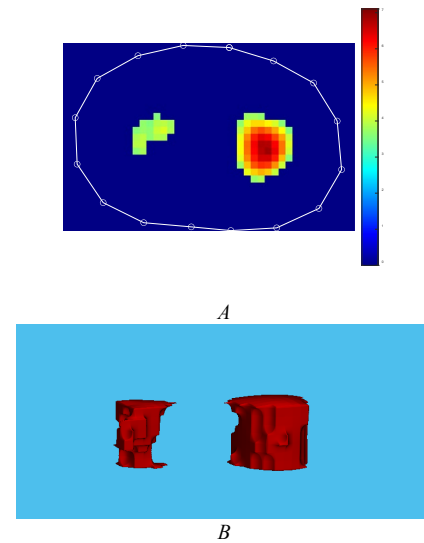


Fig.11 Left out right in, A) Image slice in midplane, B)Volume plot

A dynamical experiments showing the variation of the UST image and the UST when the right lung kept in constant air level and the air was added and removed to the left hand side lung. Fig. 12 shows one of these experiments. In this experiment, the air comes in and out to the left balloon periodically while the right balloon does not change. The mean value of the measured data differences is shown in Fig. 9.

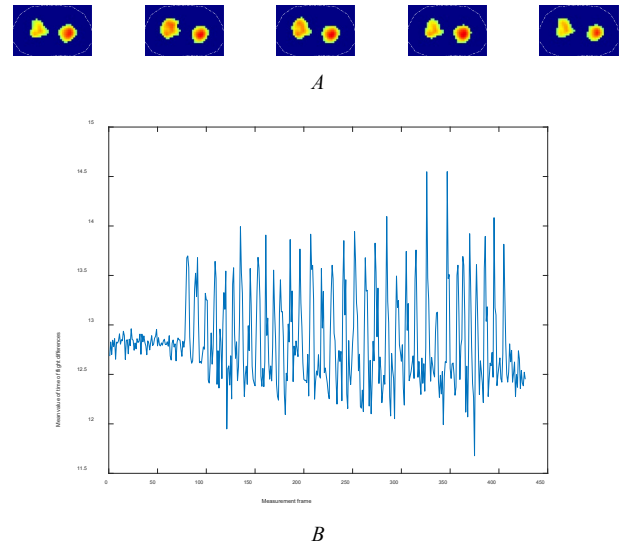


Fig. 12 Dynamical experiments, A) images from measurement frame number 78 to 82 and B) the mean value of TOF data

Several image quantification tools can be used to evaluate the performance of the UST lung imaging. This will depends on specific lung imaging applications, for example in mechanical ventilation the regional air distribution is critical. As per future clinical application the lung volume and distribution of air can be compared with respect to a reference point in breathing cycle. In Fig.8 the central inclusion was not recovered in EIT while it was reconstructed in UST. In Fig. 9, 10, 11 the image colorbar showing the indication of level of air volume. In Fig. 12 the air in and out cycle is reprsented in mean TOF data analysis.

IV. CONCLUSIONS

A geometrical representative thorax phantom was developed in this study. Both EIT and UST were used with two rings of 16 sensors. The paper focuses on the use of UST in this experimental phantom study. At the same time, we provide some indicator comparisons with the EIT imaging sensor. Static and dynamic image reconstruction was done in 3D lung imaging by filling and emptying two air balloons representing a simple breathing simulation. While the UST sensors are contactless and from outside the thorax phantom, it is worth noticing that the phantom does not include the detailed bone structure that will exist in human studies. We focus on lung function, but the UST system could be a great candidate for pulmonary function imaging, including heart function. The hope is that the paper will motivate future clinical studies to use UST as a potentially very low-cost, portable and safe imaging modality for the thoracic area. The phantom in this study does not include a model of rib bones. The influence of the ribs could lower the amplitude of the received signal on the receiver transducers. Nevertheless, reconstruction of the image would be possible. This would require additional verification through the selection of appropriate probes with the optimal frequency for humans.

Furthermore, reconstruction of the sound velocity distribution can help monitor the pulmonary system, as the sound velocity is related to the tissues' physical properties and organ function, such as airflow in the lung. In conclusion, UST can be used for lung imaging and should be able to detect the change in thorax sound velocity distribution. It will make the UST a helpful diagnostic and quantitative evaluating tool for respiratory conditions and functions. The hope is that this work will motivate future clinical studies for lung UST.

REFERENCES

- [1] C. Li, N. Duric, and L. Huang, "Comparison of ultrasound attenuation tomography methods for breast imaging," *Med. Imaging 2008 Ultrason. Imaging Signal Process.*, vol. 6920, no. March 2008, p. 692015, 2008.
- [2] L. F. Gonçalves, J. Espinoza, R. Romero, J.P. Kusanovic, B. Swope, J.K. Nien, O. Erez, E. Soto, M.C. Treadwell, "Fourdimensional ultrasonography of the fetal heart using a novel Tomographic Ultrasound Imaging display," *J. Perinat. Med.*, 34, 39–55, 2006.
- [3] A. Berzigotti, L. Castera, "Update on ultrasound imaging of liver fibrosis," *J. Hepatol.* 59, 180–182, 2013.
- [4] M. Imbault, D. Chauvet, J.L. Gennisson, L. Capelle, M. Tanter, "Intraoperative functional ultrasound imaging of human brain activity," *Sci. Rep.* 7, 7304, 2017.
- [5] T.L. Szabo, "Diagnostic Ultrasound Imaging: Inside Out," Academic Press: Cambridge, MA, USA, 2004.
- [6] B. Zhou, X. Yang, X. Zhang, W.J. Curran, T. Liu, "Ultrasound elastography for lung disease assessment." *IEEE Trans. Ultrason. Ferroelectr. Freq. Control.* 67, 2249–2257, 2020.
- [7] K. Zhang, M. Li, F. Yang, S. Xu, A. Abubakar, "Three-dimensional electrical impedance tomography with multiplicative regularization." *IEEE Trans. Biomed. Eng.* 66, 2470–2480, 2019.
- [8] D. Rueter, H.P. Hauber, D. Droeman, P. Zabel, S. Uhlig, "Low-frequency ultrasound permeates the human thorax and lung: A novel approach to non-invasive monitoring." *Ultraschall Der Med.-Eur. J. Ultrasound* 31, 53–62, 2010.
- [9] C. Li, L. Huang, N. Duric, H. Zhang, C. Rowe, "An improved automatic time-of-flight picker for medical ultrasound tomography." *Ultrasonics* 49, 61–72, 2009.
- [10] G.R. Wodicka, K.N. Stevens, H.L. Golub, E. G. Cravalho, D. C. Shannon, "A model of acoustic transmission in the respiratory system." *IEEE Trans. Biomed. Eng.* 36, 925–934, 1989.
- [11] P. Koulountzios, T. Rymarczyk, M. Soleimani, "A 4-D Ultrasound Tomography for Industrial Process Reactors Investigation," *IEEE Transactions on Instrumentation and Measurement* 71, 1-14, 2022.
- [12] M. Khairi, S. Ibrahim, M. Yunus, M. Faramarzi, G. P. Sean, J. Puspanathan, A. Abid, "Ultrasound computed tomography for material inspection: Principles, design and applications," *Measurement*, Volume 146, Pages 490-523, 2019.
- [13] C. Tan, X. Li, H. Liu, F. Dong, "An ultrasonic transmission/reflection tomography system for industrial multiphase flow imaging." *IEEE Trans. Ind. Electron.* 66 9539–9538, 2019.
- [14] H. Liu, F. Dong, Z. Li, Z. Zhang, C. Tan, "Sequential dynamic aperture focusing strategy for transmissive ultrasonic phase array tomography." *IEEE Transactions on Industrial Electronics* 69 (12), 13706-13715, 2019.
- [15] Zhang, T.; Guo, R.; Zhang, H.; Zhou, H.; Cao, Y.; Li, M.; Yang, F.; Xu, S., "Image Human Thorax Using Ultrasound Traveltime Tomography with Supervised Descent Method." *Appl. Sci.* 12, 6763, 2022.
- [16] T. Goldstein and S. Osher, "The Split Bregman Method for L1-Regularized Problems," *SIAM J. Imaging Sci.*, vol. 2, no. 2, pp. 323–343, 2009.



MANUCHEHR SOLEIMANI received the B.Sc. degree in electrical engineering and the M.Sc. degree in biomedical engineering, and the Ph.D. degree in inverse problems and electromagnetic tomography from The University of Manchester, Manchester, U.K., in 2005. From 2005 to 2007, he was a Research Associate with the School of Materials, The University of Manchester. In 2007, he joined the

Department of Electronic and Electrical Engineering, University of Bath, Bath, U.K., where he was a Research Associate and became a Lecturer, in 2008, a Senior Lecturer, in 2013, a Reader, in 2015, and a Full Professor, in 2016. In 2011, he founded the Engineering Tomography Laboratory (ETL), University of Bath, working on various areas of tomographic imaging, in particular multimodality tomographic imaging. He has authored or co-authored well over 350 publications in the field



TOMASZ RYMARCZYK Director of Research and Development centre Netrix S.A. and WSEI University. His research area focuses on application of non-invasive imaging techniques, electrical impedance tomography, image reconstruction and process tomography. Application of software engineering, AI and computerised measurement system is area of interest.